Opto-optical light deflection

Gleen T. Sincerbox, Gérald Roosen

Opto-optical light deflection

Glenn T. Sincerbox and Gerald Roosen

Light deflection is accomplished by diffraction from a transient index modulation established as a grating of variable frequency in an optical material by the interference of two controlling light beams. This device may be considered an opto-optical analog to an acoustooptical deflector, in that a change in angular deflection is created by altering the frequency of the diffraction grating. In this paper we report on a technique for altering the grating frequency by changing the wavelength of the control beams and the use of a novel optical system to maintain the Bragg condition over a wide range of frequencies. Configurations exhibiting very large angular deflections have been designed using a computer simulation and optimization program that allows minimization of the Bragg detuning. This new method of light deflection allows either discrete or continuous light scanning or modulation. A particular example using lithium niobate will be discussed which produces an 11.8° deflection from a 0.027-μm wavelength change and with an angular detuning of less than ±0.03°. The use of other materials, inorganic, organic, and dispersive, will also be discussed.

I. Introduction

The diffraction of an optical wave front resulting from its interaction with a periodic structure produces both light deflection and modulation effects and has formed the basis for many optical devices and investigative techniques. Of particular interest are those periodic structures created by optical interference methods and loosely categorized as some form of holography. This has resulted in the creation of optical elements such as diffraction gratings,[1] holographic deflection devices based on mechanical motion,[2] integrated optical modulators,[3] transient grating techniques for spectroscopic investigation,[4] and an extremely large field of activity in the general category of phase conjugation or degenerate four wave mixing.[5] In this paper we describe a novel, nonmechanical deflection (modulation) technique using diffraction from an optically generated transient standing wave to induce a periodic refractive-index variation. This is analogous to an acoustooptic device where diffraction occurs from the refractive-index modulation introduced into an optically transparent material by a traveling acoustic wave. In both cases variable deflection angles are achieved by changing the frequency of the controlling beam(s) in order to alter the spacing of the diffracting structure. In the case of opto-optical deflection, however, we have reduced Bragg detuning effects and greatly extended

the angular operating range by incorporating a real-time method to change the orientation of the diffracting structure in proper synchronization with the changing spacing. This type of device is not subject to aperture, resolution, rise-time, and chirp-distortion considerations that occur in an acoustic device and are caused by the small propagation velocity of the acoustic wave. It will, however, be necessary to develop and incorporate techniques for rapid wavelength scanning[6,7] and identify materials with high sensitivity and rapid response.

Although this application will eventually be strongly dependent on the nonlinear materials and theory associated with four wave mixing, we will not at this time treat diffraction in terms of the field radiated by the nonlinear polarization created in the medium but rather in terms of conventional holographic recording and reconstruction. In the following section we will discuss diffraction from a sinusoidal phase grating of finite thickness with emphasis on satisfying the Bragg condition by introducing a change in both grating orientation as well as frequency. Subsequent sections will examine a technique for producing these changes using conventional diffraction gratings positioned in each control beam and will utilize a model of the interference/diffraction process to describe the influence of the optical and mechanical parameters on angular deflection and Bragg detuning. Numerical examples are then presented and supported by experimental results.

II. Thick Gratings and the Bragg Effect

In this section the basic properties of thick holograms are reviewed to allow a better understanding of what will be described later. Let us consider two coherent plane waves of wavelength λ incident at angles θ_1 and θ_2 on a

Glenn Sincerbox is with IBM Research Laboratory, 5600 Cottle Road, San Jose, California 95193; G. Roosen is now with Institut d'Optique, 503 Centre Universitaire, B.P. 43 91406 Orsay, France.

recording medium of index n. These beams undergo refraction to angles ϕ_1 and ϕ_2 and interfere as shown in Fig. 1. In the thick medium the interference fringes are planes that bisect the internal angle between the wave normals of the interfering plane waves. The distance d between the crest values of intensity is related to this angle by the following relation:

$$2nd \sin\tfrac{1}{2}(\phi_1 + \phi_2) = \lambda. \tag{1}$$

Assuming that the interference pattern has been recorded inside the medium as a modification of either its refractive index or its absorption, we now illuminate this structure as shown in Fig. 2 with a beam of different wavelength λ_0. This beam will interact with the medium modulation and will be diffracted. The theory developed for thick holograms[8] has shown that, in order to get a good diffraction efficiency, the incoming beam must be incident on the grating at an internal angle satisfying the Bragg condition

$$2nd \sin\phi_0 = \lambda_0. \tag{2}$$

Varying the wavelength of the incident control beams from λ to $\lambda + \Delta\lambda$ without changing their incidence angles causes a shift in the standing wave frequency, fringe spacing d, thus giving rise to a change in the direction at which the beam at λ_0 must be incident. This angular change to the Bragg condition is simply obtained by differentiation of Eq. (2) and substituting from Eq. (1). For the case of equal angles $\phi_1 = \phi_2$, this leads to

$$\Delta\phi_0 = -\left(\frac{\Delta d}{d}\right)\tan\phi_0 = -\left(\frac{\Delta\lambda}{\lambda}\right)\tan\phi_0. \tag{3a}$$

This is shown in Fig. 3 where the λ_0 illuminating direction is maintained at the original Bragg angle of ϕ_0 and the resulting diffraction direction changes by $2\Delta\phi_0$ (to first order). Associated with this angular shift, however, will be a decrease in diffraction efficiency η as determined by coupled wave theory for a thick, phase hologram.[8] This relationship (when dealing with ferroelectric material, we must keep in mind that the value of the efficiency given by Eq. (3b) stands for certain particular cases only.[9] It has been introduced here as an easy way of understanding what is presented in the following sections) is given by

$$\eta = \frac{\exp(-i\xi)\sin(\xi^2 + \nu^2)^{1/2}}{\left(1 + \frac{\xi^2}{\nu^2}\right)^{1/2}}, \tag{3b}$$

where

$$\nu = \frac{\pi \Delta n T}{\lambda_0 \cos\phi_0}, \tag{4}$$

$$\xi = \frac{\pi T(\phi - \phi_0)}{d}, \tag{5}$$

ϕ and ϕ_0 being, respectively, the internal incidence and Bragg angles, Δn the index variation induced by the interfering beams in the medium, T the thickness of the hologram thus created, λ_0 the wavelength of the beam reading this hologram, and d the fringe spacing as given by Eq. (1). Figure 4 shows an example of how the reconstruction efficiency varies as ξ differs from zero through departure of the angle of incidence from the

$$2nd \sin \tfrac{1}{2}(\phi_1 + \phi_2) = \lambda$$
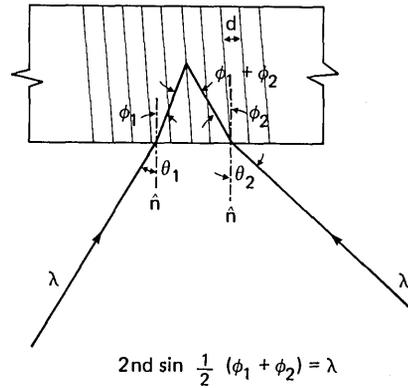
Fig. 1. Interference of two wave fronts.

$$2 n d \sin\phi_0 = \lambda_0$$

$$\frac{\lambda_0}{\sin\phi_0} = \frac{\lambda}{\sin\tfrac{1}{2}(\phi_1 + \phi_2)}$$
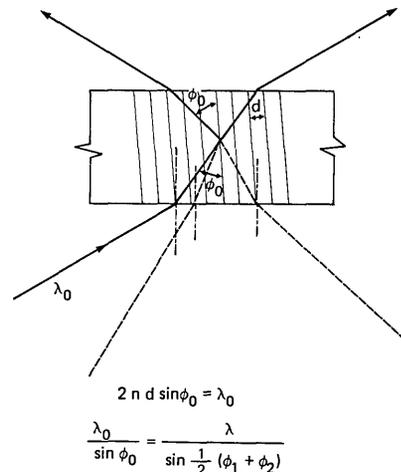
Fig. 2. Diffraction from a periodic structure.

$$\phi_0' \rightarrow \phi_0 - 2\,\frac{\Delta\lambda}{\lambda}\,\tan\phi_0$$
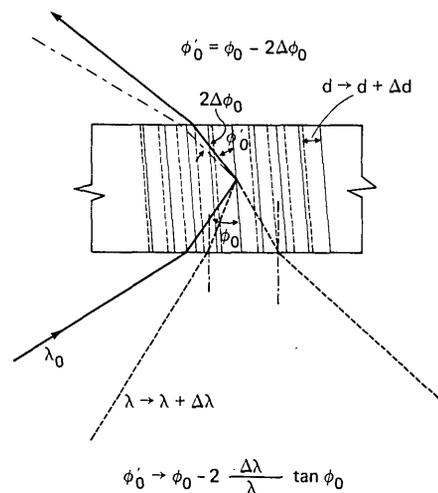
Fig. 3. Effect of a change in recording wavelength on the diffraction of an illuminating beam incident at a fixed angle.

Bragg condition. For example, if the controlling beams of wavelength 0.5 μm each make an external angle of 15° to the normal of a medium with a refractive index of 1.5, the resulting internal grating spacing is $d = 0.966\ \mu$m. An incident beam of wavelength 0.6 μm will be diffracted with maximum efficiency if it is externally in-
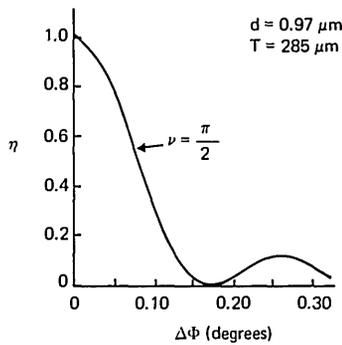
Fig. 4. Diffraction efficiency as a function of angular detuning from the Bragg condition.

cident at 18.09° [Eq. (2)], assuming no dispersion. A maximum efficiency of $\eta = 1.0$ is achieved according to Eq. (4), when $\nu = \pi/2$ or, in this case, when $\Delta n\,T = 0.293$ μm. This could be, for example, a 293-μm thick sample with index modulation of $\Delta n = 10^{-3}$ or any other combination giving the same product. For any case where $\nu = \pi/2$, the efficiency in Eq. (3b) decreases to zero when $\xi = (\sqrt{3}/2)\pi \approx 2.7$. According to Eq. (5) this could occur for a 293-μm thick sample by an actual physical change of the internal illumination angle of 0.16°. The same effect would be caused by a change in the fringe spacing that would require this amount of angular correction to be introduced in order to maintain the Bragg condition. This latter is the more realistic case for us since the illuminating beam is generally fixed in direction and the wavelength is changed to alter the fringe spacing. In this case a wavelength change of 0.007 μm would be sufficient to cause a deflection of the fixed illuminating beam by 0.32° and would result in a simultaneous decrease of the diffraction intensity to zero. For more weakly diffracting materials, i.e., $\Delta n \sim 10^{-4}$, the thickness must be increased to 2.93 mm with an associated increase in angular sensitivity to 0.016°. For this thicker material a corresponding wavelength change of 0.0007 μm would decrease the diffraction to zero. The modulation slope for a given wavelength variation will be adjustable through the selection of the thickness of the periodic structure which governs the Bragg selectivity by Eq. (5).

III. Light Modulation

If we consider the zero order, creating, suppressing, or altering the periodic structure in the medium in this manner will serve as a gate to modulate the incident beam and allow either the transformation of a cw incident beam into a pulsed transmitted one or the modification of the shape and/or the length of an incident pulsed wave front. Using pulsed pump beams for creating the periodic structure will also allow very short pulses to be obtained, particularly if their arrival times are properly phased with the incident beam and with each other. The main advantage of this opto-optical method of modulation is that the optical wave propagates through the medium at the speed of light and imposes no aperture vs response time restriction. The modulation speed is restricted to the speed at which
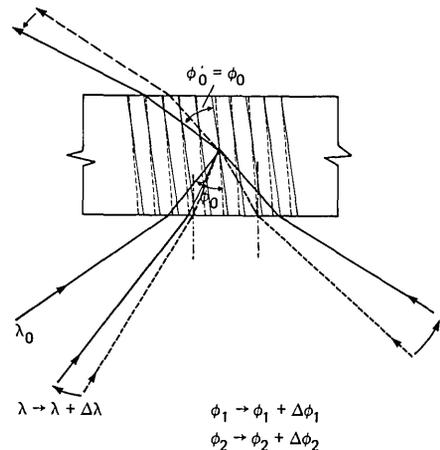
wavelength can be turned on or off or shifted and the lifetime of the effect causing the refractive-index modulation (e.g., population inversion, photobleaching, liquid crystal reorientation, drift or photoexcited electrons, charge transfer). Wavelength changes of over 0.015 μm can be rapidly created on a nanosecond time scale by intracavity tuning of a cw dye laser[6] or in the case of GaAs lasers at picosecond speeds by altering the drive current.[7]

IV. Light Deflection

As pointed out in Sec. II, varying the frequency of the standing wave changes not only the diffracted angle of the third beam but drastically decreases the diffraction efficiency because of Bragg detuning. To achieve light deflection over a sufficiently large angular range without serious loss in efficiency, we therefore need a technique to keep the Bragg condition satisfied. This can be accomplished as shown in Fig. 5 by simultaneously changing both the orientation and frequency of the standing wave in a predetermined manner. In this way an incoming light beam having a fixed incident direction would always satisfy the Bragg condition.

To achieve this simultaneous change in both the frequency and the orientation of the standing wave while varying the wavelength of the two writing beams, we have conceived a passive technique that operates in real time over a wide angular deflection range. This is shown in Fig. 6 where the incoming beam is split into the two identical writing beams by a beam splitter each of which are incident on dispersive media, in this case diffraction gratings G_1 and G_2. Changing the wavelength of the incident beam causes a change in the direction of the diffracted beams and consequently a change in the direction of the beams incident on the recording medium. Using different spatial frequencies the change in each beam can be different and we therefore should expect a simultaneous change in both the spacing and the direction of the standing wave. Although it is also possible to use a single unique sinusoidal grating without a beam splitter and the +1 and −1 orders obtained after diffraction of the incident beam, we will describe in what follows only the case of
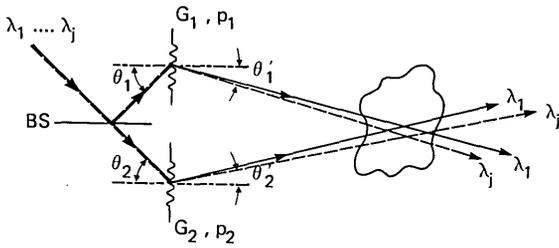
$$\sin \theta_i' = \frac{m_i \lambda_j}{p_i} - \sin \theta_i$$

Fig. 6. Method for creating wavelength-dependent changes in incidence angles using diffraction gratings.
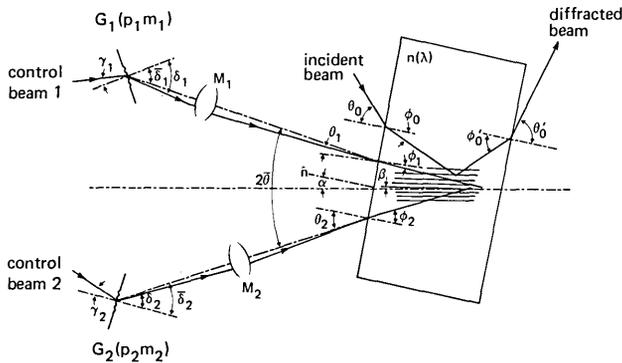
Fig. 7. Geometry describing parameters for fringe recording and beam diffraction.

using two gratings having different spatial frequencies.

Using optical systems that image the grating plane onto the sample plane, the diffracted beams can be directed to overlap in the medium in which the standing wave has to be recorded whatever the incident wavelength. In the case of an afocal system, collimation is maintained for the beams incident onto both the gratings and the medium. This point has importance, as we will indicate later.

In reference to Fig. 7, assume that each afocal system has an angular magnification M_i ($i = 0,1,2$) where the subscripts 1 and 2 are used to denote each of the writing beams and the subscript 0 is the illuminating beam. The incidence angle onto the medium is such that the angle between these beams is given by $2\bar{\theta}$. These incidence angles are defined for the mean wavelength $\bar{\lambda}$ within the tuning range and establish two optical axes, one for each afocal system, and is the direction about which the individual beam direction will vary as the wavelength changes. That is, when the incident beams are at wavelength $\bar{\lambda}$ they will travel along the axis of each system, and as the wavelength changes the beam paths will depart from the axis and the variation in the incidence angles will undergo magnification. The combination of differences in grating period and optical magnification will cause each writing system to react differently to the same wavelength shift and thereby cause an asymmetry in the incidence angles and a tilting of the planes. The task is to select parameters that minimize the Bragg detuning over the entire range of wavelength variation.

The set of equations that govern the incident and diffracted directions, θ_{0j} and θ_{0j}', of the illuminating beam of wavelength λ_0 that is interacting with the grating formed at wavelength λ_j can be derived as follows. Light incident on grating G_i at the mean wavelength $\bar{\lambda}$ in the writing wavelength range is diffracted into a direction $\bar{\delta}_i$ according to

$$\sin \bar{\delta}_i = \frac{m_i}{p_i} \bar{\lambda} - \sin \gamma_i, \qquad (6)$$

where γ_i is the angle of incidence onto grating G_i, m_i is the diffraction order, and p_i is the grating period. The diffraction direction at any over wavelength λ_j is

$$\sin \delta_{ij} = \frac{m_i}{p_i} \lambda_j - \sin \gamma_i. \qquad (7)$$

The angle of incidence of the beams of wavelength λ_j with respect to the sample normal for an afocal system aligned along $\bar{\delta}_i$ is given by

$$\theta_{ij} = \bar{\theta} + M_i(\delta_{ij} - \bar{\delta}_i) - \alpha, \qquad (8)$$

where α is the inclination of the medium surface normal with respect to the bisector of the two writing beam optical systems. These beams are refracted at the surface, and by Snell's law the internal angles ϕ_{ij} for isotropic media are given by

$$\phi_{ij} = \sin^{-1} \frac{1}{n_j} \sin \theta_{ij}, \qquad (9)$$

where n_j is the refractive index of the medium subscripted for wavelength in the event that dispersion is present. The resulting grating spacing of the interference pattern is, according to Eq. (1),

$$d_j = \frac{\lambda_j}{2 n_j \sin \frac{1}{2}(\phi_{1j} - \phi_{2j})}. \qquad (10)$$

The tilt of the planes is given by

$$\beta_j = -\frac{1}{2}(\phi_{1j} + \phi_{2j}) \qquad (11)$$

and is measured with respect to the normal to the sample surface. The internal directions of the incident and diffracted beams, ϕ_{0j} and ϕ_{0j}', of wavelength λ_0 that satisfy the Bragg condition are given by

$$\phi_{0j} = -\beta_j + \sin^{-1} \frac{\lambda_0}{2 d_j n_0}, \qquad (12)$$

$$\phi_{0j}' = -\beta_j - \sin^{-1} \frac{\lambda_0}{2 d_j n_0}, \qquad (13)$$

where n_0 is the refractive index at λ_0 of the medium. The external incidence and diffraction angles, θ_{0j} and θ_{0j}', are by Snell's law:

$$\theta_{0j} = \sin^{-1} n_0 \sin \phi_{0j}, \qquad (14)$$

$$\theta_{0j}' = \sin^{-1} n_0 \sin \phi_{0j}'. \qquad (15)$$

For each wavelength λ_j in the tuning range and for a given parameter set, these equations are solved for the external incidence and diffraction angles of the illuminating wave that satisfy that particular Bragg condition. The maximum deviation of the incidence angles from a constant direction is determined for the entire set, and, if this is greater than a predetermined Bragg detuning limit, a parameter change is introduced and a

new calculation performed. Iteration on the parameter set continues in an attempt to bring the detuning angle below limit. At this point the maximum deflection angle is determined by comparing the diffraction angle θ'_{0j}.

Our experience has been that the parameter set p_i, M_i, $\bar\theta$, and α is sufficient to always provide a solution for which the detuning is small. The choice of tilt angle α is dependent on the cut and orientation of the crystal being examined which must be selected to maximize the induced nonlinearity for efficient operation.

V. Numerical Example

As an example consider a system for deflecting a He–Ne laser beam, 0.633 μm, that uses the fixed argon laser lines between 0.477 and 0.514 μm as the controlling wavelength—analogous to a digital deflector. If the individual writing beams use gratings of periods $p_1 = 1.695$ μm and $p_2 = 0.715$ μm, and diffraction orders of $m_1 = +1$ and $m_2 = +1$, an optical system with equal angular magnification of $M_1 = M_2 = 0.5$ in each beam will produce variations in the incidence angles of 0.65° and 1.62°, respectively, for the 0.038-μm wavelength change. These angles are determined from Eq. (8) and measured with respect to the individual optical axes that have been aligned using the 0.501-μm wavelength as the mean wavelength λ. The difference in angular spread between the two beams results from the difference in input grating dispersions. It is this ultimate angular difference that tilts the recorded fringes to maintain the Bragg condition.

Table I shows the effect of changing the angle between the individual optical axes as they illuminate the medium. This angle determines the operating point, bias, about which the spacing of the periodic structure varies in response to the wavelength-induced angular shifts. In this example the normal to the medium is aligned to bisect the angle between the optical axis, i.e., the sample is not tilted. The calculations are performed using LiNbO$_3$ as the test medium $n = 2.29$. For axis aligned at ±8.0° a deflection angle in excess of 2.5° can be obtained for the 0.038-μm wavelength shift. There is significant Bragg detuning in the amount of 0.28° such that if the average incidence angle is fixed at 10.19° the resulting variation of ±0.14° would result in a serious mismatch in the Bragg condition and significant loss in deflection efficiency. Decreasing the angle of the optical axis to ±5.0° causes only a slight decrease in overall deflection angle, ≈2.3°, and has a significant

Fig. 8. Effect of control beam incidence angle on both Bragg detuning and deflection angle for one particular configuration.

effect on the Bragg detuning. This decrease is by an order of magnitude and such that an average incidence angle of 6.333° will experience only a ±0.014 mismatch with only a slight loss in diffraction efficiency (see Fig. 4). This reduction in Bragg detuning with incidence angle suggests the existence of an optimum operating point for a given set of parameters. Such an optimum does indeed exist and is shown in Fig. 8 where both the Bragg detuning and maximum deflection angle are plotted vs incidence angle. All other parameters are the same as mentioned above except for sample tilt which has been changed to $\alpha = -1.6°$ to produce the best minimum. In this particular case the minimum occurs for a ±5.15° optical axis orientation and has a detuning angle of 0.021°. The corresponding deflection is 2.27° and appears to be linear over this range of incidence angles. It should be noted that a similar behavior can be generated at any angle of incidence by appropriately adjusting the angular spread of control light through selection of grating dispersion and/or magnification parameters.

For the optimum angular alignment, the influence of sample tilt is shown in Fig. 9 where the illuminating incidence angle that satisfies the Bragg condition is plotted as a function of control wavelength. The solid curve represents the above determined tilt of $\alpha = -1.6°$ and the broken curves are for deviations of ±10° from this orientation. The effect is small with the most noticeable effect being a shift in the location of the minimum. Within a fixed wavelength range it can be observed that the smallest variation in incidence angle occurs when the curve is centered about the mean wavelength used to define the optical axis in each beam.

The influence of different materials with different refractive indices has also been examined using the above optimum configuration. The calculated Bragg detuning corresponding to later experiments for these materials, bismuth silicon oxide (Bi$_{12}$SiO$_{20}$ or BSO), lithium niobate (LiNbO$_3$), and ruby, are 0.025°, 0.022°, and 0.022°, respectively. The corresponding deflection angles are all 2.27°. It should be emphasized that for these data the configuration for BSO was optimized to minimize the Bragg detuning and it is this configuration

Table I. Calculated Reconstruction Angles Satisfying the Bragg Condition for Two Orientations of the Control Beam Optical Axis Using LiNbO$_3$

Control beam Wavelength (μm)	Illuminating beam (0.633 μm)			
	Incident angle (degrees) axis = ±8.0°	Deflected angle (degrees)	Incident angle (degrees) axis = ±5.0°	Deflected angle (degrees)
0.477	10.331	−11.770	6.331	−7.764
0.488	10.227	−11.007	6.318	−7.096
0.497	10.155	−11.396	6.319	−6.559
0.501	10.128	−11.128	6.322	−6.322
0.515	10.048	−9.204	6.348	−5.506
$\Delta = 0.038$	$\Delta = 0.283$	$\Delta = 2.566$	$\Delta = 0.029$	$\Delta = 2.258$

Fig. 9. Variation of Bragg detuning with wavelength for three different sample orientations.

Fig. 10. Diffraction efficiency and deflection angle comparison of fringe tilting (solid curve) and static fringe (broken curve) light deflectors.

that is used for the other materials. If these were to be minimized on their own their detuning could be significantly reduced. In this we see that for this configuration there is no significant difference in the Bragg detuning angle and subsequent maximum deflection angle in spite of the differences in refractive indices $n = 1.77$ for ruby and 2.29 for LiNbO₃ or the presence of dispersion $2.8 > n > 2.5$ as in the case of BSO.[10] The above calculations were performed at a relatively low spatial frequency, 360 mm⁻¹, and hence the small angular deflection of 2.27°. By increasing the spatial frequency of the optically generated standing wave to 2000 mm⁻¹ (using incidence angles of ±30° at 0.501 μm), the resulting deflection for a 0.488–0.515-μm wavelength shift increases significantly to 11.9°. To maintain the Bragg condition over this large angular range the angular spread should be increased by increasing the magnification in each of the afocal optical systems by a factor of 7 to $M_1 = M_2 = 3.5$. The corresponding Bragg detuning over this range is calculated to be $\Delta\theta \cong 0.06°$ and hence efficient operation is anticipated. Even at these larger angles the effect is essentially independent of the recording medium.

The effectiveness of this fringe tilting technique in maintaining high reconstruction efficiency over a broad deflection range is graphically illustrated in Fig. 10. The curves show the calculated variation in efficiency and deflection angle as a function of an extended wavelength range centered at 0.501 μm. The high spatial frequency configuration described above was used to generate data representing deflection with and without wavelength-induced tilting. For the tilting case, represented by the solid curves, a single illumination angle was selected from the solution set of Eq. (14) and the internal Bragg angle mismatch computed at each control wavelength using

$$\Delta\phi_j = \sin^{-1}\left(\frac{\lambda_0}{2n_0 d_j}\right) - \sin^{-1}\left[\frac{1}{n_0}\sin(\phi - \alpha)\right] - \beta_j, \qquad (16)$$

and the results inserted into the coupled wave efficiency expression, Eq. (3b). The corresponding deflection angle variation is a plot of Eq. (13). For the nontilting case, broken curves, the results were generated by replacing, mathematically, the gratings with mirrors and hence removing all wavelength dependence from the incidence angle of the control beams. This, in essence,
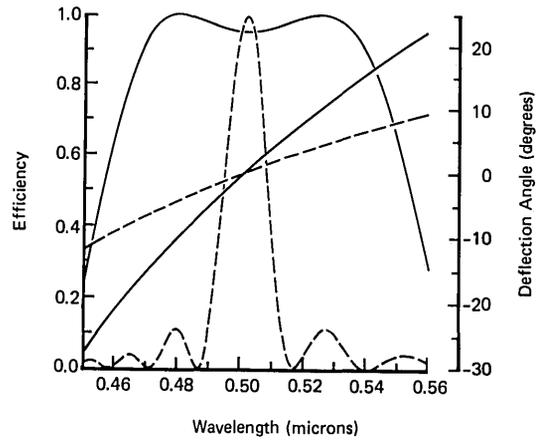
is the same as using Eq. (3a) for the angular mismatch of a conventional Bragg device. The deflection in this case is equal to $2\Delta\phi$ corrected for refraction (to first order). As is quite evident in the figure, the fringe tilting technique produces a significant improvement in both deflection angle sensitivity and uniform efficiency. For this particular example the full-width-half-power tuning range increases from 0.014 to 0.097 μm and, more importantly, the deflection angle increases by more than 1 order of magnitude from 2.6° to 43.6°. For a given wavelength tuning range the deflection sensitivity increases from 185 to 450°/μm.

VI. Experimental Implementation

Before realizing the dispersive fringe tilting technique we demonstrated the validity of our theoretical analysis using separate components to act on each of the discrete wavelengths in the argon set. As can be expected, this was quite cumbersome, difficult to align, and not easily changed. It was, however, adequate to demonstrate our process and provide motivation to continue. The basic setup for generating both low and high spatial frequency standing waves using the fringe tilting technique is shown in Fig. 11. In these first experiments we used an argon laser and a beam splitter BS to create the two writing beams that were directed onto two reflection gratings G_1 and G_2 with periods of 1.695 and 0.715 μm, respectively. A_1 and A_2 are two imaging afocal systems with magnification that can be independently varied thus allowing a change in the ultimate dispersion in the overlapping volume where the recording medium is located. This system also enables us to vary the diameter of the interfering field at the sample. In the current experiments this diameter was varied from 0.5 to 10 mm. The difference between the path lengths of the two writing beams was maintained to a distance smaller than the laser coherence length. The probe beam to be deflected came from an He–Ne laser and was directed to be incident at the calculated Bragg angle for the standing wave created at the mean writing wavelength, usually 0.501 μm. The variation in direction of the deflected red beam resulting from a change in the wavelength of the writing beams was determined by

Fig. 11.   Experimental arrangement.
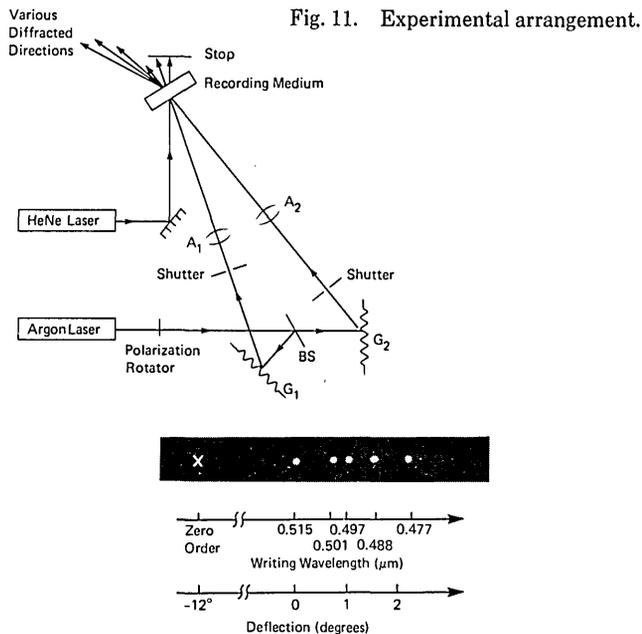
Fig. 12.   Deflected 0.633-μm light using five argon laser wavelengths for control at a low spatial frequency (358 mm^{-1}) in LiNbO$_3$.

Table II.   Comparison of Calculated and Measured Deflection Angles for LiNbO$_3$ Using a Low Spatial Frequency Deflection 358 mm^{-1}

Writing beam wavelength shift (μm)	Illuminating beam (0.633 μm) deflection angle (degrees)	
	calculated	measured
0.477–0.515	2.27°	2.28°
0.488–0.515	1.60°	1.60°
0.497–0.515	1.06°	1.05°

either running the argon laser single line and rotating the selective prism inside the cavity to select each line independently or running it all lines and therefore displaying as many deflected red beams as writing wavelengths. In this later case, the resultant efficiency is lower due to the competition process between the various induced gratings. After having measured the variation of the direction of the diffracted beam and determined the writing and erasing sensitivity and the diffraction efficiency, the diffracted spots were photographically recorded.

VII.   Results and Discussion

Although we have performed our experiments with several crystals on hand, including LiNbO$_3$, BSO, and ruby, the majority of our work has been with LiNbO$_3$. It was not always possible to use the BSO crystal particularly for certain spatial frequencies of the induced standing wave. Indeed without the use of an external applied electric field this crystal does not record correctly a low frequency standing wave.[11] During these experiments the dependence of the diffraction efficiency on the direction of polarization of the incident beams on the recording material orientation was again noticed[12] and will be the subject of a later paper.

The results of low spatial frequency recording, 358 mm^{-1} (optical axis at ±5.15°), using the parameters of Table I and the configuration of Fig. 11, are shown in

Table III.   Comparison of Calculated and Measured Deflection Angles for LiNbO$_3$ Using a Medium Spatial Frequency Deflection 745 mm^{-1}

Writing beam wavelengths (μm)	Illuminating beam (0.633 μm)		measured deflection (degrees)
	calculated detuning (degrees)	deflection (degrees)	
0.477	0.040	2.52	2.52
0.488	0.006	1.06	1.01
0.497	0.000	0.00	0.00
0.502	0.005	−0.64	−0.68
0.515	0.040	−2.18	−2.23
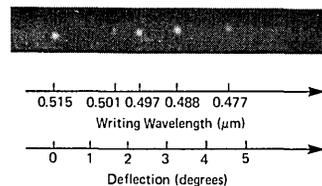
Fig. 13.   Deflected 0.633-μm light using five argon laser wavelengths for control at a medium spatial frequency (745 mm^{-1}) in LiNbO$_3$.

Table IV.   Comparison of Calculated and Measured Deflection Angles for a High Spatial Frequency Deflection 2000 mm^{-1}

Sample type	orientation (degrees)	Writing beam wavelength shift (μm)	Illuminating beam (0.633 μm) deflection angle (degrees)	
			calculated	measured
LiNbO$_3$	−6.35°	0.488–0.515	11.76	11.75
BSO	−1.06°	0.488–0.515	11.87	11.88

Table II for both LiNbO$_3$ and ruby. The precision on the angular measurement for all data presented is ±0.02°. Excellent agreement is achieved between experiment and calculations. At this spatial frequency the total deflection is 2.28° for the 0.038-μm wavelength shift—a sensitivity of 60°/μm. Figure 12 is a photograph showing these five diffracted positions for 0.633-μm illumination.

The angular Bragg sensitivity was determined for our 5.0-mm thick LiNbO$_3$ sample. At this frequency the half-power width is ~0.08° and hence our calculated Bragg detuning of $\Delta\theta = 0.01°$ has a negligible effect on the reconstruction efficiency. Without the fringe tilting method the Bragg detuning over this range of wavelength change would be $\Delta\theta \sim 0.25°$ [Eq. (3a)], and the efficiency would decrease to zero.

At higher spatial frequencies, $\bar{\nu} = 745$ mm^{-1}, 21.4° between beam axis, the angular magnification of the afocal systems was increased by a factor of 2 and the results are shown in Table III for LiNbO$_3$. The deflections are normalized to the center wavelength 0.497 μm and can be seen to be 4.7° or 124°/μm twice as large as the previous case. The angular detuning is also larger, ±0.020°, but still sufficient to maintain high efficiency. The resulting five spots of deflected 0.633-μm light are presented in the photograph of Fig. 13.

Finally, Table IV shows the results for both BSO and LiNbO$_3$ at the highest spatial frequency tested, 2000 mm^{-1}. In this case the afocal angular magnification was increased to 3.5. The angular deflection has been

(a)

(b)

0.515 ——————— 0.488
Writing Wavelength (μm)

0 ——————— 12°
Deflection (degrees)
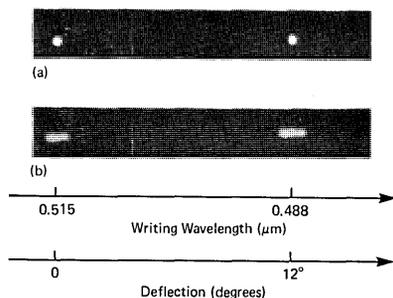
Fig. 14. Deflected 0.633-μm light using two argon laser wavelengths for control at a high spatial frequency (2000 mm^{-1}) in LiNbO$_3$: (a) using an afocal control beam; (b) using a conjugate image control beam system.

significantly increased to 11.8° (435°/μm), while maintaining a workable Bragg detuning of $\Delta\theta$ = 0.030°.

If instead of using the afocal collimating system in each of the control beams we use a conjugate imaging system, the section of the diffracted beam is no longer circular. This comparison is shown in Fig. 14 where (a) are the spots from an afocal system using collimated beams and (b) are spots from an imaging system where only the input is a collimated beam. This is understandable if one considers the shape and spatial frequency distribution of the hologram induced in the material by the two interfering beams. As these beams are now converging beams the spatial frequency of the diffracting periodic structure seen by the third beam while propagating in the medium varies from one side to the other thus causing this observed dispersion in the direction of diffraction.

VIII. Summary

We have demonstrated the possibility of deflecting (modulating) an optical beam utilizing an optically induced periodic structure. Through the use of a novel fringe tilting technique, extremely large angular deflections have been demonstrated while simultaneously maintaining the Bragg condition necessary for uniform diffraction efficiency over the deflection range. This large deflection range coupled with no aperture restrictions, except those related to material power density considerations and hence deflection speed, leads us to expect that a deflector with >10^4 spots per field can be realized ($N = D\Delta\theta/\lambda$, where D is the aperture).

This study was conducted using inorganic materials for the purpose of demonstrating the process and many other materials are certainly applicable. The diffraction efficiency obtained with our particular sample of LiNbO$_3$ was of the order of 1%, and the response time when operating in cw mode with 100-mW cm^{-2} power densities was very slow. An opto-optical deflector using this recording material should be used with pulsed lasers in order to have very short response time. On the other hand, a high energy density is easily obtained from low power sources in guided structures. For example, an optically generated standing wave in a LiNbO$_3$ waveguide with a solid state laser would allow real-time performance as either a purely optical gate or a modulator[3] for a beam interacting with that structure.

Furthermore if we use our Bragg correction we could realize either a continuous or multispot light deflector according to the kind of wavelength variation chosen. BSO being much more sensitive than LiNbO$_3$ allows a reduction in the writing energy response time, but a dc electric field must be applied to obtain an acceptable diffraction efficiency. Barium titanate (BaTiO$_3$), which has been successfully used in four wave mixing experiments[13] could lead to a higher diffraction efficiency by virtue of its larger electrooptic coefficient. This in turn allows the use of a thinner medium, a relaxed Bragg condition, and hence a larger deflection angle. The speed of response of this material is intermediate between BSO and LiNbO$_3$ and subject to the same inverse relationship to control beam power density. In ruby the problems are similar but in addition the millisecond lifetime of the triplet state limits the response time of the material as far as the decay of the induced grating is concerned. We also observed a dramatic change in diffraction efficiency over the range of wavelengths used in our experiments that can be attributed to nonuniform wavelength response of ruby.[14]

It is considered very likely that organic materials may have even greater potential in implementing a practical device.[15] The probability is very high that an appropriate organic molecule can be identified or engineered that will combine high sensitivity to permit the use of low power lasers for controlled operation and, at the same time, a fast index modulation mechanism to allow high speed deflection performance.[16] A further goal would be to seek a material with spectral sensitivity in the near infrared in order to use the high speed wavelength scanning techniques associated with current tuned solid state lasers.

References

1. G. Pieuchard and J. Flamand, Jpn. J. Appl. Phys. 14, Suppl. 14-1 (1975).
2. L. D. Dickson, G. T. Sincerbox, and A. D. Wolfheimer, IBM J. Res. Dev. 26, 228 (1982).
3. R. P. Kenan, D. W. Vahey, N. F. Hartman, V. E. Wood, and C. M. Verber, Opt. Eng. 15, 12 (1976); W. S. Goruk, P. J. Vella, R. Normandin, and G. I. Stegeman, Appl. Opt. 20, 4024 (1981).
4. D. W. Phillion, D. J. Kuizenga, and A. E. Siegman, Appl. Phys. Lett. 27, 85 (1975).
5. S. M. Jensen and R. W. Hellwarth, Appl. Phys. Lett. 32, 167 (1978); A. Yariv, IEEE J. Quantum Electron. QE-14, 650 (1978); C. R. Giuliano, Phys. Today, 27 (Apr. 1981).
6. J. M. Telle and C. L. Tang, Appl. Phys. Lett. 26, 572 (1975).
7. J. M. Osterwalder and B. J. Rickett, IEEE J. Quantum Electron. QE-16, 250 (1980); B. Pokrowsky and G. C. Bjorklund, IBM San Jose Research; private communication.
8. H. Kogelnik, Bell Syst. Tech. J. 48, 2909 (1969).
9. N. V. Kukhtarev, V. B. Markov, S. G. Odulov, M. S. Soskin, and V. L. Vinetskii, Ferroelectrics 22, 949 (1979).
10. R. E. Aldrich, S. L. Hou, and M. L. Harvill, J. Appl. Phys. 42, 493 (1971).
11. J. P. Huignard, J. P. Herriau, G. Rivet, and P. Günter, Opt. Lett. 5, 102 (1980).
12. F. S. Chen, J. Appl. Phys. 40, 3389 (1969).
13. J. Feinberg and R. W. Hellwarth, Opt. Lett. 15, 519 (1980).
14. P. F. Liao and D. M. Bloom, Opt. Lett. 3, 4 (1978).
15. Y. Silberberg and I. Bar-Joseph, Opt. Commun. 39, 265 (1981).
16. A. F. Garito and K. D. Singer, Laser Focus, 59 (Feb. 1982).